Reconfiguration of Multistable 3D Ferromagnetic Mesostructures Guided by Energy Landscape Surveys

Yi Li[a1], *Samuel J. Avis*[b1], *Junbo Chen*[c], *Guangfu Wu*[a], *Teng Zhang*[c,d]*, *Halim Kusumaatmaja*[b]*, *Xueju Wang*[a,e]*

[a]Department of Materials Science and Engineering, University of Connecticut, Storrs, CT 06269, USA

[b]Department of Physics, Durham University, Durham, DH1 3LE, England

[c]Department of Mechanical and Aerospace Engineering, Syracuse University, Syracuse, NY, 13244, USA

[d]BioInspired Syracuse, Syracuse University, Syracuse, NY 13244, USA

[e]Institute of Materials Science, University of Connecticut, Storrs, CT 06269, USA

[1]These authors contributed equally to this work.

*Corresponding authors. Email: xueju.wang@uconn.edu; halim.kusumaatmaja@durham.ac.uk; tzhang48@syr.edu

Abstract

Three-dimensional (3D) mesostructures that can reversibly change their geometries and thereby their functionalities are promising for a wide range of applications. Despite intensive studies, the lack of fundamental understanding of the highly nonlinear multistable states existing in these structures has significantly hindered the development of reconfigurable systems that can realize rapid, well-controlled shape changes. Herein we exploit systematic energy landscape analysis of deformable 3D mesostructures to tailor their multistable states and least energy reconfiguration paths. We employ a discrete shell model and minimum energy pathway methods to establish design phase diagrams for a controlled number of stable states and their energy-efficient reconfiguration paths by varying essential geometry and material parameters. Concurrently, our experiments show that 3D mesostructures assembled from ferromagnetic composite thin films of diverse geometries can be rapidly reconfigured among their multistable states in a remote, on-demand fashion by using a portable magnet, with the configuration of each stable state well maintained after the removal of the external magnetic field. The number of stable states and reconfigurable paths observed in experiments are in excellent agreement with computational predictions. In addition, we demonstrate a wide breadth of applications including reconfigurable 3D light emitting systems, remotely-controlled release of particles from a multistable structure, and 3D structure arrays that can form desired patterns following the written path of a magnetic "pen". Our results represent a critical step towards the rational design and development of reconfigurable structures for applications including soft robotics, multifunctional deployable devices, and many others.

1. Introduction

Reconfigurable three-dimensional (3D) structures that can actively change their geometries and thereby their functionalities upon external stimuli (like mechanical forces, magnetic fields, hydration, and temperature) (1-6) are promising for a diverse range of applications including deployable solar panels (7), metamaterials (8-10), phononics (11, 12), biomedical devices (13, 14), robotics (15-17), metasurfaces (18, 19), and many others. The design of reconfigurable structures usually relies on structural instabilities (20-22), stimuli-responsive constituent materials (like swellable gels, shape memory polymers and magnetic materials) (5, 23-26), or their heterogeneous combinations (27). For example, origami and kirigami, ancient art of folding of 2D thin sheets along predefined creases to create 3D objects, have been widely used as platforms for deployable structures due to their multiple deployed stable states under mechanical deformation (28-32). Structural instabilities have also been exploited in recently developed mechanics-guided assembly approaches to complex 3D functional architectures and electronics in a diversity of configurations and a broad range of material compositions (33-37). Through elastically deforming the assembly platform in different time sequences (i.e., loading-path control), the 3D architectures and electronics can morph into different shapes (38, 39). In addition to mechanical deformation and associated structural stability, reconfigurable structures can also be realized through active constituent materials including ferromagnetic composites (4, 40-42), hydrogels (5), shape memory polymers (SMPs) (6, 35), liquid crystal elastomers (LCEs) (43), and electrochemically active materials (44), which can change their shape upon external stimuli.

In recent years, an emerging attractive strategy to realize robust reconfigurable structures is to encode multiple stable states by design without the need for persistent external stimuli (45-48). Each stable state is a local minimum in a high-dimensional and complex energy landscape, and hence only a temporal external stimulus is needed to guide the structure to

traverse from one local minimum to another. Despite intensive studies, a number of critical challenges remain, especially when asymmetric and complicated modes are involved in the architectural reconfiguration. The first challenge is associated with the presence of multiple local minimum configurations, which could affect the stability of the targeted stable state under perturbations (e.g., environmental noises) or trap the structure in an intermediate state during the process of reconfiguration. For example, it is recently recognized by researchers that hidden local minimum configurations can destroy the designed pathway of deploying origami structures (49-51). Thus, it is crucial to provide means of manipulating the energy well depth of targeted configurations and eliminating unfavorable local minima in the design of reconfigurable structures. The second challenge stems from the complexity of the transition paths from one local minimum state to another, especially when the two states are separated by other stable and transition states (52-56). A recent work (56) shows that the transition from a uniformly deformed cylindrical shell to a 9-dimple buckled pattern needs to pass 7 local minimum configurations, which cannot be achieved by directly applying local probes to the shell. Complicated transition paths among local minima are also found in mechanical metamaterials, which further provides new design parameters to program the deformed configurations of the structures (55). Finally, it is also very challenging to realize remote, locally controlled, and rapid reconfiguration of the deformed, highly nonlinear structures (38, 57). These challenges call for a new means of systematically surveying the energy landscapes of the multistable structures to probe and tailor the energy barrier height among different local minima.

Here we present a set of strategies and design concepts to address these challenges using a tightly integrated experimental and theoretical approach. 3D mesostructures assembled from ferromagnetic composite thin films via mechanical buckling (33) are used as a model system to conduct the study. By leveraging active magnetic materials, we show that remote

reconfiguration among different stable states is achieved rapidly and on demand via a portable magnet. The use of magnetic actuation eliminates the need for mechanical stages to apply a global deformation to the substrate of the 3D mesostructures, thus providing opportunities for remote, tetherless shape morphing. Theoretically, we employ a discrete shell model (58, 59) and pathfinding algorithms (56, 60) to conduct fundamental studies on the complicated energy landscapes of the 3D ferromagnetic structures. We construct design phase diagrams showing how the available stable states sensitively depend on the essential material and geometrical parameters of the elastic structures. Furthermore, energy-efficient reconfiguration paths between the stable states and their energy barriers are identified using a combination of the string method (60) and our developed binary image transition state search method. A salient advantage of our approach is that it allows the computation of reconfiguration paths following the minimum energy pathways (MEPs) systematically without the need to assume a predefined path for the structural transformation. Our methodology is versatile and is applied to design and realize reconfigurable structures with a wide range of geometries, including ribbons and structures that resemble tables, baskets, flowers, boxes, single and double beams. In all cases, the theoretically predicted and experimentally realized shapes and reconfiguration paths are in excellent agreement. We also demonstrate reconfiguration of structures fabricated from non-active materials that are locally patterned with ferromagnetic films, which significantly expands the design space and material libraries for reconfigurable structures.

To further highlight the versatility of our reconfigurable 3D ferromagnetic structures, we also demonstrate a number of applications. Reconfigurable light emitting systems illustrate the capacity to integrate other materials and functional components into the 3D structures. Magnetically actuated particle delivery in different modes of a table structure and reconfigurable ferromagnetic structure arrays that can display well-controlled patterns formed by reconfiguring the structures following the written path of a magnetic “pen”, serve as additional examples of reconfigurable systems.

2. Results

Design phase diagram of multistable states of magnetically reconfigurable 3D mesostructures

Figure 1a schematically illustrates the assembly process of a 3D structure from ferromagnetic composite thin films via compressive buckling, and the architectural reconfiguration of the structure via magnetic actuation. The ferromagnetic composite is prepared by homogeneously embedding hard NdFeB (neodymium-iron-boron) microparticles with an average diameter of 5 μm into a soft elastomer, polydimethylsiloxane (PDMS) (**Figure S1**). NdFeB is chosen for our study because its high residual magnetic flux density over a wide range of applied magnetic fields allows complex modes of reconfiguration(4). The assembly of 3D ferromagnetic structure starts with patterning the ferromagnetic composite thin films into 2D layouts using a CO_2 laser (VLS 3.50, University Laser System, Norman, OK), followed by their axial magnetization using impulse magnetic fields (about 2.7 T) generated by an impulse magnetizer. The 2D patterns are then laminated onto a prestretched elastomer (Dragon skin, Smooth-on, Chicago, IL), with a very thin layer of superglue applied at selective locations (bonding sites) of the 2D patterns to generate strong bonding between the pattern and the elastomer substrate. The interfacial interactions at all other locations are dominated by comparatively weak van der Waals forces. Releasing the prestrain in the substrate leads to compressive forces on the 2D ferromagnetic pattern at the bonding sites and geometrically transforms the pattern into a 3D structure through controlled compressive buckling. Throughout the paper, we always position the 2D layout on the x-y plane so that its normal vector is in the z direction.

Figure 1b presents experimental and corresponding computational results of a 3D ferromagnetic table structure (film thickness: 150 μm) and its multiple stable states. The table structure is oriented in a way such that gravity is perpendicular to the substrate (in the negative

z direction), which is the case for most of the structures in this study unless specified otherwise. To efficiently explore the possible stable states existing in the table structure, we use a discrete shell model (see details in Supplementary Note 1 in the Supporting Information) to locate the stable configurations, where the energy of the buckled structures is locally minimized. Three distinct states (state 1-3) with a total of nine configurations are discovered. Magnetically deforming the assembled table structure via a portable disk magnet (Neodymium magnet, K&J Magnetics), with one leg becoming flat while the other three legs being in a buckled status, rapidly reconfigures the table structure from state 1 into a distinct stable state 2, with four configurations corresponding to different orientations (state 2: shape I-IV). Further magnetic actuation induces an additional leg of the table structure to become flat and results in the transition from state 2 into another stable state with four different orientations (state 3: shape I-IV). A key benefit of using such rapid, remote, on-demand magnetic actuation is that it eliminates the need for manipulating mechanical stages or other tethered techniques to induce the morphing of 3D structures as used in previous works (38, 39), which is advantageous for many applications, especially those that require deployment and shape morphing in enclosed or delicate environments such as robotics and biomedical devices. In addition, unlike previously reported reconfigurable 3D structures that rely on persistent external stimuli to maintain their deformed shapes (4, 5, 43, 61), the deformed configurations of the table structure shown here can well maintain their shapes after the applied magnetic field is removed, as they are locally stable configurations. Computational modeling results of the configurations for the stable states and their different orientations via the discrete shell model are highly consistent with experiments, with the color in the results denoting the displacement of the structure along the z direction.

Using the combined experimental and computational strategy, we further study the effect of essential geometry and material properties on the entire spectrum of existing stable states, yielding the design phase diagram shown in **Figure 1c**. The diagram illustrates the total

number of stable states according to two dimensionless parameters that are determined from the ratios between three relevant energy scales – gravitational (E_G), stretching (E_S), and bending (E_B). These energy scales can be expressed in terms of the material and geometric parameters of the 3D structure:

$$E_G = \rho g L^3 t,$$

$$E_S = E L^2 t,$$

$$E_B = \frac{E t^3}{1 - \nu^2},$$

where ρ is the material density, E is the Young's modulus, ν is the Poisson ratio, t is the film thickness, and L represents the in-plane size of the structure (the width of table legs is used for this study). The cubic term of L in E_G comes from the fact that the volume of the structure scales with L^2 and the displacement in the direction of gravity is proportional to L. Three regimes in terms of the number of existing stable states can be identified in **Figure 1c**: (i) 3 distinct stable states, (ii) 2 distinct stable states, and (iii) 1 distinct stable state, which are controlled by two dimensionless variables $E_S/E_B = L^2(1-\upsilon^2)/t^2$ and $E_G/E_B = \rho g L^3(1-\upsilon^2)/Et^2$. The variable E_S/E_B characterizes the bendability of the structure, with a larger value indicating that it is easier to generate bending deformation. E_G/E_B describes the competition between the gravitational and bending energies. When E_S/E_B and E_G/E_B are relatively large, three distinct stable states as shown in Figure 1b exist in regime i, with states 2 and 3 having 4 different orientations. As the two dimensionless variables decrease, state 2 becomes unstable, resulting in two distinct stable states (states 1 and 3) for regime ii. When E_G/E_B is further reduced to an even smaller value, only the buckled-up state (state 1) is stable in regime iii. To validate the phase diagram experimentally, we fabricate 3D ferromagnetic structures of the same film thickness (t = 125 μm) and material properties (ρ, E, and ν) but of different sizes (L), and magnetically reconfigure them into their multistable states. **Figure 1d** (i-iii) demonstrates the number and configurations of the stable states for structures with L = 1.04 mm, 0.8 mm, and

0.5 mm, respectively, which agree well with the prediction of the design phase diagram. Please note that the overall in-plane dimensions of the structures are scaled proportionally with L as it varies. The diagram provides very important guidelines for achieving a well-controlled number of stable states or for removing undesired stable states in various applications by tuning the geometry and material properties. For instance, if state 2 is undesired, the structure can be designed with E_S/E_B and E_G/E_B falling within regime ii, where only states 1 and 3 are stable.

Reconfiguration paths among distinct stable states of 3D ferromagnetic mesostructures

Identifying the optimal transition pathways between the stable states of a 3D structure is critical for well-controlled, energy-efficient reconfigurations. By using the table structure as an example, we further examine its energy landscape to identify the so-called minimum energy pathways (MEPs), corresponding to steepest-descent pathways between metastable states, in which the maximum energy along the path occurs at a saddle point (the transition state). Our approach allows automatic and systematic computation of reconfiguration paths following the MEPs without the need to assume the pathways along which the structure morphs. This is useful because the energy-efficient reconfiguration paths can be highly complex for 3D elastic structures, and it is not always possible to prescribe an expected pathway *a priori*, as typically adopted in previous works where energy barriers are calculated (31, 38, 53, 62).

As shown in **Figure 2a**, we find the transition pathways to progress from state 3 to state 1 of the table structure can be broadly grouped into three regions: (I) two paths, path 1 and path 2, exist (red region); (II) two paths, path 1 and path 2*, exist (orange region); (III) only path 1 exists (yellow region). The difference between paths 2 and 2* is that a stable state 2 only exists on path 2. For illustration, we construct the design diagram by varying the in-plane size of the structures (L), while keeping their material properties (ρ , E, and ν) and film thickness (t=125 μm) constant. The marked red and blue points correspond to those in the 3-state and 2-state regimes identified in the design diagram in **Figure 1c**, respectively.

For L > 0.89 mm (region I), two independent minimum energy pathways are found and illustrated in **Figure 2b** for a representative table structure with L = 1.04 mm: a direct pathway, with energy barrier ΔE_1 (path 1), and a path that passes through state 2 (point D in **Figure 2b**) as an intermediary, with energy barriers ΔE_2 between states 3 and 2 and ΔE_3 between states 2 and 1 (path 2). Snapshots of configurations along the pathways are captured in simulations and magnetic reconfiguration experiments and are shown in **Figure 2b,** with the complete structural transformation process and corresponding energy profiles simultaneously demonstrated in **Supplementary Movies 1 and 2**. The energy barriers of the pathways demonstrate both the stability of the states and the ease of transitioning between them. For example, the energy barrier to progress from state 3 to state 1 is much smaller than that from the inverse direction, thereby making state 1 more stable. Comparing paths 1 and 2 also suggests that a smaller input energy is needed when reconfiguring the table structure along path 2 (passing two saddle points) than that along path 1. However, the finite energy barrier ΔE_3 also indicates that the transition can be potentially trapped in state 2 if insufficient external energy is provided for reconfiguration. In addition, reconfiguration along path 2 requires more efforts in manipulating the direction and the strength of external magnetic forces, compared to the direct pathway following path 1. These complexities clearly show the importance of harnessing the energy landscape analysis for guiding the choice of transition paths based on specific applications and the nature of available external magnetic fields (or other external stimuli). In addition, it is also worth noting that the pathways observed in experiments, where a portable magnet is utilized to reconfigure the structure from state 3 to state 1, are highly consistent with those from simulations, which indicates the high fidelity and reliability of the approach used in this study. Moreover, the reconfigurations in our experiment can be completed within a few seconds (**Supplementary Movies 1 and 2**). Such fast and remotely controlled transitions are desired for numerous applications, such as in soft robotics (63, 64) and multifunctional metasurfaces (18, 19).

As we decrease L, all the energy barriers become smaller monotonically, as shown in **Figure 2a**. At L = 0.89 mm, the boundary between the 3-state and the 2-state regimes in the phase diagram of **Figure 1c** is reached, where ΔE_3 reduces to zero, a signature that state 2 is no longer stable. For 0.78 mm < L < 0.89 mm (region II in **Figure 2a**), there remains two distinct minimum energy pathways to transition from state 3 to state 1, even in the absence of a stable state 2. The typical energy profiles for this range of L values are illustrated in **Figure 2c** for L = 0.80 mm. Snapshots of the configurations from simulations and experiments for L = 0.80 mm are further shown in **Figure 2c**, with reconfiguration along the full pathways provided in **Supplementary Movies 3 and 4**. The shape evolution along the pathways remains qualitatively similar to that shown in **Figure 2b**. Interestingly, we also find that there is a crossover in the preferred energy-efficient pathway at L = 0.84 mm, where $\Delta E_1 = \Delta E_2$ in **Figure 2a**. For a larger L (0.84 mm < L < 0.89 mm), path 2* is favorable because the corresponding energy barrier is smaller, while for a smaller L (0.78 mm < L < 0.84 mm), path 1 has a lower energy barrier and thereby is desired.

The preference for path 1 at smaller L values is further accentuated by the loss of path 2* as a minimum energy pathway for 0.56 mm < L < 0.78 mm (region III in **Figure 2a**). For this range of L values, we are unable to identify path 2* in simulations, as indicated by the lack of data points in **Figure 2a**. The absence of path 2* is further demonstrated by our failure to experimentally reconfigure the table structure along this pathway using the portable disk magnet (see **Supplementary Movie 5**), unlike the case for larger L values. Here, only path 1 remains. The typical energy profile for the transition along path 1 in this range of L values is shown in **Figure 2d** for L = 0.72 mm, with the corresponding snapshots of the reconfiguration and the full pathway given in **Figure 2d** and **Supplementary Movie 6**, respectively.

State 3 itself becomes unstable when L is further reduced below 0.56 mm, where we enter the 1-state regime. At this point, we cross the phase boundary between the 2-state and 1-state regimes in **Figure 1c**, and the energy barrier ΔE_1 becomes zero in **Figure 2a**. Taken

together, these highly nonlinear behaviors observed for the transition pathways make the energy landscape analysis a necessary tool for an efficient and robust design of the multistable configurations and the transition paths among them, which has not been systematically studied before for continuous 3D mesostructures. In addition, we perform experimental studies of reconfiguring the table structure between its state 1 and state 3 for 100 times. The results show high repeatability (Figure S2). Investigating the repeatability above 100 times of reconfiguration and the associated fatigue behaviors of the structure is not within the scope of the work and warrants further study.

Reconfigurable 3D ferromagnetic structures of diverse geometries

The reconfiguration strategy and the energy landscape analysis described above are versatile and can be extended to different types of 3D structures in diverse geometries, as illustrated in **Figures 3**. **Figure 3a and Figure S3** show an assembled ferromagnetic basket structure (shape I; film thickness: 125 μm) and its multiple stable states (shapes II-IV) that can be achieved via magnetic control. The pink arrows indicate differences among the four shapes. In addition, by introducing creases to selective locations of a ribbon structure (crease thickness: 70 μm; non-crease thickness: 125 μm), we create a ferromagnetic origami structure, which is further tuned to display multiple stable configurations by using magnetic forces.

The elastomer substrate used for 3D assembly in **Figure 1**, **Figure 2** and **Figure 3a** provides essential support for the assembled 3D structures, but it also poses some limitations for the reconfiguration in the out of plane direction. To allow more freedom for spatial reconfiguration, the substrate underneath the 3D table structure is removed, while the substrate adjacent to the bonding sites is maintained to support the 3D structure (see **Figure S4**). Such 3D structure on a hollow substrate allows bending up/down deformations across the plane of the substrate. **Figure 3b** and **Figure S5** demonstrate a rich library of reconfigurable 3D

structures on hollow substrates, including basket, single- and double-beam structures, as well as their distinct, multistable shapes.

It is very interesting to note that the multistable configurations on hollow substates are sensitive to the orientation of the structures. Take the table structure for example, it is shown that the structure only displays two stable states, buckled up and down states, when placed horizontally (i.e., the direction of gravity is perpendicular to the in-plane direction of the substrate, **Figure S5**d). However, when the table structure is placed vertically with the direction of gravity in the *x* direction (**Figure 3b**), in addition to the buckled up (Shape I) and down (Shape IV) states, it can deform into an asymmetric, twisted shape (Shape II), similar to state 3 of the table structure with an intact substrate. This deformed shape can be further magnetically deformed into shape III, with the four bonding sites attached to the substrate and the rest of the structure self-supported in the air. We also carry out energy landscape analysis for this structure, the details of which are presented in **Figure S6**. Similar to the case with an intact substrate, we can distinguish several regimes with different numbers of stable states, depending on the three relevant energy scales: gravitational, stretching, and bending energies. In addition, we quantitatively compare the dimensions of three representative 3D structures from experiments and modeling results and find negligible difference between them (Table S1), which further highlights the consistency between modeling and experimental results. It is worth noting that the mechanics-guided buckling technique and magnetic actuation can enable the fabrication and manipulation of reconfigurable 3D structures, as shown in previous works(33, 65). However, minimization of reconfigurable structures is not the scope of this work and will be pursued elsewhere."

Reconfigurable 3D hybrid structures

In addition to tuning the strength and the direction of external magnetic forces for reconfiguration, an alternative and potentially more versatile means to realize magnetically

controlled reconfiguration is through manipulating the distribution of magnetic materials within 3D hybrid structures. **Figure 4a** schematically illustrates the fabrication process of such structures by locally integrating laser-cut ferromagnetic composite film patches (125 μm thick) onto a thin layer of inactive materials (PDMS, 180 μm thick) and compressively buckling the 2D hybrid pattern into a 3D structure. Following this strategy, reconfigurable 3D hybrid structures that resemble tables and flowers are fabricated and magnetically tuned to display five stable configurations (Shape I-V) using a portable magnet. The deformed shapes can well maintain their configuration after the magnetic force is removed, the capability of which is the same as structures composed of a single layer of ferromagnetic composites. 3D Hybrid structures at a smaller length scale can be potentially achieved by directly patterning bilayer or multilayer 2D hybrid structures using the raster mode of a laser or reactive ion etching to remove ferromagnetic films at undesired regions. The fabrication technique of hybrid structures allows the integration of almost any class of materials with active components (like magnetic films), which significantly expands the design space and accessible constituent materials of the reconfigurable structures. In addition, 3D hybrid structures can potentially allow more local magnetic control by varying the direction and the strength of the residual magnetic field in each ferromagnetic patch through magnetization in different directions and mixing different concentrations of magnetic particles in the composite film, respectively. However, the exploration of other composition materials for reconfigurable 3D hybrid structures and variation in the magnetic direction and strength are not within the scope of this work and will be pursued elsewhere.

Applications of reconfigurable 3D structures

Integrating functional materials and components onto 2D ferromagnetic composite patterns provides immediate access to tunable 3D functional devices. As an example, we demonstrate reconfigurable light emitting systems in **Figure 5a**. The fabrication begins with

the integration of two light emitting diodes (LEDs) with a dimension of 1 mm ×0.4 mm×0.2 mm onto designated locations of a double-beam structure. Copper thin films (thickness: 60 μm) connected to the two poles of the LED serve as interconnects for subsequent LED activation. Formation of 3D architectures from these 2D functional precursors follows the 3D buckling schemes introduced earlier. Magnetically tuning the assembled 3D structure to deform from shape I to II (or III) enables a firm contact between the two poles of the LED (located at one beam) with two corresponding copper films (on the substrate) that are connected to an external power supply for power input, and therefore activates the LED. Furthermore, the LED can maintain its "on" status after the magnetic force is removed due to the stability of the deformed configurations (shapes II and III). When the two beams are simultaneously deformed to form stable configuration IV using a magnet, both LEDs are turned on. This simple example suggests a broad range of possibilities in other types of electronic and optoelectronic devices.

Based on the magnetically actuated reconfiguration strategy, we also assemble a 3D structure in a table shape for the delivery of particles in a well-controlled manner. As shown in **Figure 5b** and **Figures S7**, the structure is composed of ferromagnetic composite films (thickness: 180 μm) and a thin layer of pure PDMS film (thickness: 60 μm) in a concave shape as the table face, where a silica particle is placed for the demonstration. To trigger the delivery of the particle, a portable magnet is manipulated to actuate the deformation of the structure into multistable configurations of four different orientations (modes I-IV), leading to well-controlled particle delivery in different directions. The layout of the hybrid ferromagnetic table structure allows the table face that supports the particle to stay insensitive to the applied magnetic field when the table structure is magnetically actuated, thereby exerting minimal influence on the reconfiguration of the whole structure. Such flexible, remotely reconfigurable structures have a lot of potential applications in controlled delivery.

To demonstrate the scalability of the fabrication process as well as more capabilities of reconfigurable structures, we assemble a 4×4 array of reconfigurable table structure units with

a unit size of 3×3 mm^2 (**Figure 6a**). Each structure unit has the identical original shape, as shown in the magnified image a-i in Figure 6. Actuating the 3D structure array following a defined trajectory with a portable magnet consecutively and rapidly reconfigures the 3D structures along the path into deformed shapes (image a-ii), which are maintained after the magnet passes. Following different trajectories leads to various magnetically drawn patterns, like the "V" and line patterns shown in **Figure 6a** and **Figure S8**, respectively. Each structure unit is allocated sufficiently far from each other to avoid interference during magnetic actuation. **Figure 6b** shows a 4×5 array of table structures on hollow substrates. The structures are reconfigured from their "popped down" configuration (image b-i) to "popped up" state (image b-ii) following the trajectory of the magnet to display desired patterns like letter "M" (**Supplementary Movie 7**).

Discussion

To conclude, we have tightly integrated experiments and modelling to survey the energy landscapes of highly nonlinear 3D ferromagnetic structures for the development of reconfigurable systems. Our systematic computational analysis predicts a design phase diagram for a targeted number of stable states by varying essential material properties and geometries. It also allows us to systematically identify highly complex transition paths among the distinct stable states that minimize the energy barriers, without the need to prescribe an expected pathway for structural transformations *a priori*. These predictions are thoroughly validated by our experiments of creating multistable 3D ferromagnetic structures and magnetically reconfiguring the structures among their multistable states following different pathways rapidly, in a remote, on-demand manner. Using this strategy, a plethora of symmetric and asymmetric 3D mesostructures of diverse geometries are realized and reconfigured among their multistable states, including those that resemble ribbons, tables, baskets, flowers, boxes, single and double beams. Furthermore, the integration of electronic components onto ferromagnetic composites

provides immediate access to reconfigurable 3D functional devices, which is demonstrated in reconfigurable light emitting systems. The development of the magnetically actuated table structure for particle delivery and arrays of reconfigurable 3D structures that are deformed consecutively to display desired patterns highlight capabilities of potential relevance to smart, remotely controlled soft robotics and reconfigurable metasurfaces.

We believe our fundamental studies on the reconfiguration of 3D structures establish the foundations for robust and reproducible architectural reconfiguration behaviors. More broadly, our integrated experimental and modelling approach can be extended to the design and development of diverse types of reconfigurable structures and systems, including origami, kirigami and stimuli-responsive structures beyond magnetic actuation, where the exploration of energy landscapes for well-controlled reconfiguration and the tunability of multistable states are needed. It is also interesting to explore the integration of functional materials with locally patterned magnetic films of different magnetization directions (4, 64), and stiffness manipulation (66) to expand on the materials library and design space of possible hybrid structures and to potentially enable multi-stimuli-responsive structures and soft machines. We believe these studies will provide important insights for the design of reconfigurable structures and functional systems for wide-ranging applications, such as in deployable solar panels, phononics, morphable architected materials, and soft robotics.

Materials and Methods

Experiments. Details of the fabrication and reconfiguration of 3D ferromagnetic structures and devices appear in the Supporting Information.

Modeling. Details of the discrete shell model and algorithms of finding the stable states and the reconfiguration pathways are in the Supporting Information.

Acknowledgements

We acknowledge the support of the following grants: NSF-CMMI-2020676 (X.W.), NSF-CMMI-2020476 (T. Z.). S.J.A. is supported by a studentship from the Engineering and Physical Sciences Research Council (EPSRC). Simulations were performed at the facilities of the Hamilton HPC Service of Durham University and the Comet cluster (Award TG-MSS170004 to T.Z.) in The Extreme Science and Engineering Discovery Environment.

Competing interests

The authors declare no competing financial interests.

References

1. J. T. B. Overvelde, J. C. Weaver, C. Hoberman, K. Bertoldi, Rational design of reconfigurable prismatic architected materials. *Nature* **541**, 347-352 (2017).
2. E. T. Filipov, T. Tachi, G. H. Paulino, Origami tubes assembled into stiff, yet reconfigurable structures and metamaterials. *Proceedings of the National Academy of Sciences* **112**, 12321-12326 (2015).
3. M. Wehner *et al.*, An integrated design and fabrication strategy for entirely soft, autonomous robots. *Nature* **536**, 451-+ (2016).
4. Y. Kim, H. Yuk, R. Zhao, S. A. Chester, X. Zhao, Printing ferromagnetic domains for untethered fast-transforming soft materials. *Nature* **558**, 274-279 (2018).
5. A. S. Gladman, E. A. Matsumoto, R. G. Nuzzo, L. Mahadevan, J. A. Lewis, Biomimetic 4D printing. *Nat Mater* **15**, 413-+ (2016).
6. T. Xie, Tunable polymer multi-shape memory effect. *Nature* **464**, 267-270 (2010).
7. D. Thesiya, A. Srinivas, P. Shukla, A novel lateral deployment mechanism for segmented mirror/solar panel of space telescope. *Journal of Astronomical Instrumentation* **4**, 1550006 (2015).
8. Y. H. Fu *et al.*, A Micromachined Reconfigurable Metamaterial via Reconfiguration of Asymmetric Split‐Ring Resonators. *Advanced Functional Materials* **21**, 3589-3594 (2011).
9. Z. Wang *et al.*, Origami‐based reconfigurable metamaterials for tunable chirality. *Advanced Materials* **29**, 1700412 (2017).
10. K. H. Lee, K. Yu, A. Xin, Z. Feng, Q. Wang, Sharkskin-Inspired Magnetoactive Reconfigurable Acoustic Metamaterials. *Research* **2020** (2020).
11. S. Babaee, J. T. B. Overvelde, E. R. Chen, V. Tournat, K. Bertoldi, Reconfigurable origami-inspired acoustic waveguides. *Sci Adv* **2** (2016).

12. B. Deng, P. Wang, V. Tournat, K. Bertoldi, Nonlinear transition waves in free-standing bistable chains. *Journal of the Mechanics and Physics of Solids*, 103661 (2019).
13. A. Damdam, N. Qaisar, M. M. Hussain, Honeycomb-serpentine silicon platform for reconfigurable electronics. *Applied Physics Letters* **115**, 112105 (2019).
14. P. L. Anderson, A. W. Mahoney, R. J. Webster, Continuum Reconfigurable Parallel Robots for Surgery: Shape Sensing and State Estimation With Uncertainty. *Ieee Robot Autom Let* **2**, 1617-1624 (2017).
15. N. Plitea, D. Lese, D. Pisla, C. Vaida, Structural design and kinematics of a new parallel reconfigurable robot. *Robot Cim-Int Manuf* **29**, 219-235 (2013).
16. Y. Tang, Y. Li, Y. Hong, S. Yang, J. Yin, Programmable active kirigami metasheets with more freedom of actuation. *Proceedings of the National Academy of Sciences* **116**, 26407-26413 (2019).
17. B. Gorissen, D. Melancon, N. Vasios, M. Torbati, K. Bertoldi, Inflatable soft jumper inspired by shell snapping. *Science Robotics* **5** (2020).
18. K. Liu, T. Tachi, G. H. Paulino, Invariant and smooth limit of discrete geometry folded from bistable origami leading to multistable metasurfaces. *Nat Commun* **10** (2019).
19. Q. Wang *et al.*, Optically reconfigurable metasurfaces and photonic devices based on phase change materials. *Nature Photonics* **10**, 60 (2016).
20. Z. Chen *et al.*, Nonlinear geometric effects in mechanical bistable morphing structures. *Physical review letters* **109**, 114302 (2012).
21. Y. Jiang, L. M. Korpas, J. R. Raney, Bifurcation-based embodied logic and autonomous actuation. *Nat Commun* **10**, 1-10 (2019).
22. A. Zareei, B. Deng, K. Bertoldi, Harnessing transition waves to realize deployable structures. *Proceedings of the National Academy of Sciences* **117**, 4015-4020 (2020).
23. A. Lendlein, H. Y. Jiang, O. Junger, R. Langer, Light-induced shape-memory polymers. *Nature* **434**, 879-882 (2005).
24. J. Kim, J. A. Hanna, M. Byun, C. D. Santangelo, R. C. Hayward, Designing responsive buckled surfaces by halftone gel lithography. *Science* **335**, 1201-1205 (2012).
25. L. S. Novelino, Q. Ze, S. Wu, G. H. Paulino, R. Zhao, Untethered control of functional origami microrobots with distributed actuation. *Proceedings of the National Academy of Sciences* **117**, 24096-24101 (2020).
26. J. Liu *et al.*, Dual-Gel 4D Printing of Bioinspired Tubes. *ACS Applied Materials & Interfaces* **11**, 8492-8498 (2019).
27. Z. Ding *et al.*, Direct 4D printing via active composite materials. *Sci Adv* **3** (2017).
28. E. A. Peraza-Hernandez, D. J. Hartl, R. J. Malak, D. C. Lagoudas, Origami-inspired active structures: a synthesis and review. *Smart Mater Struct* **23** (2014).
29. J. L. Silverberg *et al.*, Using origami design principles to fold reprogrammable mechanical metamaterials. *Science* **345**, 647-650 (2014).
30. S. Li, H. Fang, K. W. Wang, Recoverable and Programmable Collapse from Folding Pressurized Origami Cellular Solids. *Physical Review Letters* **117** (2016).
31. H. B. Fang, K. W. Wang, S. Y. Li, Asymmetric energy barrier and mechanical diode effect from folding multi-stable stacked-origami. *Extreme Mech Lett* **17**, 7-15 (2017).
32. Y. Yang, M. A. Dias, D. P. Holmes, Multistable kirigami for tunable architected materials. *Phys Rev Mater* **2** (2018).
33. S. Xu *et al.*, Assembly of micro/nanomaterials into complex, three-dimensional architectures by compressive buckling. **347**, 154-159 (2015).

34. Y. H. Zhang *et al.*, A mechanically driven form of Kirigami as a route to 3D mesostructures in micro/nanomembranes. *P Natl Acad Sci USA* **112**, 11757-11764 (2015).
35. X. J. Wang *et al.*, Freestanding 3D Mesostructures, Functional Devices, and Shape-Programmable Systems Based on Mechanically Induced Assembly with Shape Memory Polymers. *Advanced Materials* **31** (2019).
36. K. I. Jang *et al.*, Self-assembled three dimensional network designs for soft electronics. *Nat Commun* **8** (2017).
37. W. Lee *et al.*, Two-dimensional materials in functional three-dimensional architectures with applications in photodetection and imaging. *Nat Commun* **9** (2018).
38. H. R. Fu *et al.*, Morphable 3D mesostructures and microelectronic devices by multistable buckling mechanics. *Nature Materials* **17**, 268-+ (2018).
39. W. B. Pang *et al.*, Electro-mechanically controlled assembly of reconfigurable 3D mesostructures and electronic devices based on dielectric elastomer platforms. *Natl Sci Rev* **7**, 342-354 (2020).
40. Y. Kim, G. A. Parada, S. D. Liu, X. H. Zhao, Ferromagnetic soft continuum robots. *Science Robotics* **4** (2019).
41. W. Q. Hu, G. Z. Lum, M. Mastrangeli, M. Sitti, Small-scale soft-bodied robot with multimodal locomotion. *Nature* **554**, 81-85 (2018).
42. M. Boncheva *et al.*, Magnetic self-assembly of three-dimensional surfaces from planar sheets. *P Natl Acad Sci USA* **102**, 3924-3929 (2005).
43. T. J. White, D. J. Broer, Programmable and adaptive mechanics with liquid crystal polymer networks and elastomers. *Nat Mater* **14**, 1087-1098 (2015).
44. X. X. Xia *et al.*, Electrochemically reconfigurable architected materials. *Nature* **573**, 205-+ (2019).
45. Y. P. Song *et al.*, Additively manufacturable micro-mechanical logic gates. *Nat Commun* **10** (2019).
46. H. Yang, L. Ma, Multi-stable mechanical metamaterials by elastic buckling instability. *J Mater Sci* **54**, 3509-3526 (2019).
47. M. P. O'Donnell, M. Towes, R. M. J. Groh, I. V. Chenchiah, Exploring Adaptive Behavior of Non-linear Hexagonal Frameworks. *Front Mater* **7** (2020).
48. Y. Li, S. Pellegrino, A Theory for the Design of Multi-Stable Morphing Structures. *J Mech Phys Solids* **136** (2020).
49. J. H. Na *et al.*, Programming reversibly self‐folding origami with micropatterned photo‐crosslinkable polymer trilayers. *Advanced Materials* **27**, 79-85 (2015).
50. J. L. Silverberg *et al.*, Origami structures with a critical transition to bistability arising from hidden degrees of freedom. *Nature materials* **14**, 389 (2015).
51. Z. R. Zhai, Y. Wang, H. Q. Jiang, Origami-inspired, on-demand deployable and collapsible mechanical metamaterials with tunable stiffness. *P Natl Acad Sci USA* **115**, 2032-2037 (2018).
52. R. M. J. Groh, A. Pirrera, On the role of localizations in buckling of axially compressed cylinders. *P Roy Soc a-Math Phy* **475** (2019).
53. E. Virot, T. Kreilos, T. M. Schneider, S. M. Rubinstein, Stability Landscape of Shell Buckling. *Phys Rev Lett* **119** (2017).
54. J. Marthelot, F. L. Jimenez, A. Lee, J. W. Hutchinson, P. M. Reis, Buckling of a Pressurized Hemispherical Shell Subjected to a Probing Force. *J Appl Mech-T Asme* **84** (2017).
55. E. Medina, P. E. Farrell, K. Bertoldi, C. H. Rycroft, Navigating the landscape of nonlinear mechanical metamaterials for advanced programmability. *Phys Rev B* **101** (2020).

56. J. Panter, J. Chen, T. Zhang, H. Kusumaatmaja, Harnessing energy landscape exploration to control the buckling of cylindrical shells. *Communications Physics* **2**, 1-9 (2019).
57. G. Q. Luo *et al.*, Mechanics of bistable cross-shaped structures through loading-path controlled 3D assembly. *J Mech Phys Solids* **129**, 261-277 (2019).
58. H. Seung, D. R. Nelson, Defects in flexible membranes with crystalline order. *Physical Review A* **38**, 1005 (1988).
59. E. Grinspun, A. N. Hirani, M. Desbrun, P. Schröder (2003) Discrete shells. in *Proceedings of the 2003 ACM SIGGRAPH/Eurographics symposium on Computer animation* (Citeseer), pp 62-67.
60. E. Weinan, W. Ren, E. Vanden-Eijnden, Simplified and improved string method for computing the minimum energy paths in barrier-crossing events. *Journal of Chemical Physics* **126**, 164103 (2007).
61. E. Hajiesmaili, D. R. Clarke, Reconfigurable shape-morphing dielectric elastomers using spatially varying electric fields. *Nat Commun* **10**, 183 (2019).
62. X. Shang, L. Liu, A. Rafsanjani, D. Pasini, Durable bistable auxetics made of rigid solids. *Journal of Materials Research* **33**, 300-308 (2018).
63. Y. Tang *et al.*, Leveraging elastic instabilities for amplified performance: Spine-inspired high-speed and high-force soft robots. *Sci Adv* **6**, eaaz6912 (2020).
64. Y. Alapan, A. C. Karacakol, S. N. Guzelhan, I. Isik, M. Sitti, Reprogrammable shape morphing of magnetic soft machines. *Sci Adv* **6**, eabc6414 (2020).
65. J. Cui *et al.*, Nanomagnetic encoding of shape-morphing micromachines. *Nature* **575**, 164-168 (2019).
66. Z. Zhai, Y. Wang, K. Lin, L. Wu, H. Jiang, In situ stiffness manipulation using elegant curved origami. *Sci Adv* **6**, eabe2000 (2020).

Figures

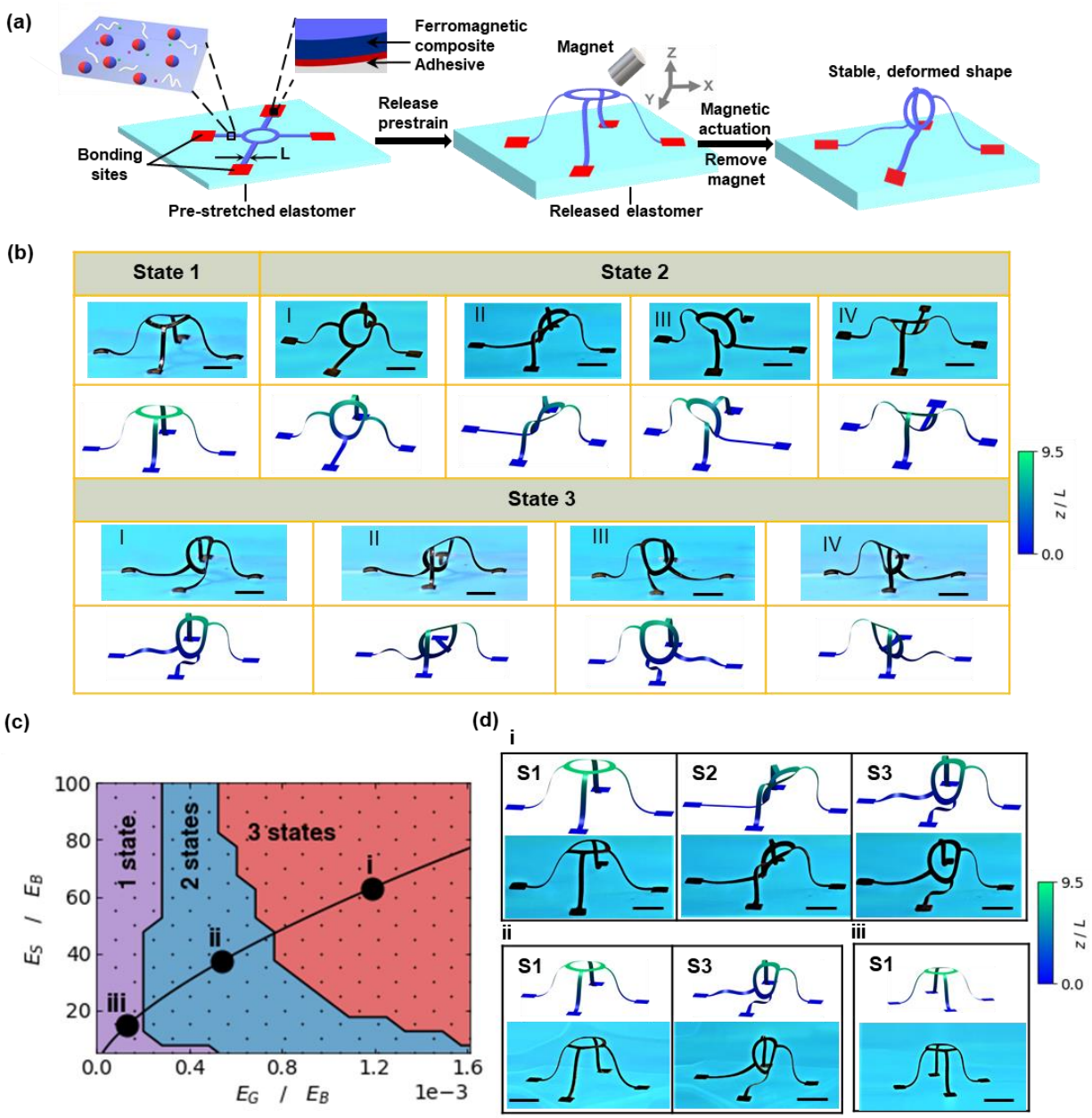

Figure 1. Multistability of magnetically reconfigurable 3D structures. (a) Schematic illustration of the assembly and reconfiguration schemes of 3D ferromagnetic structures. **(b)** Experimental and computational results of multistable states coexisting in a 3D table structure. Scale bars, 1 cm. **(c)** Design phase diagram showing the number of distinct stable states based on the energy scales of the table structure. The three marked points denote representative examples in each regime. **(d)** Experimental and computational results of the distinct stable states existing in three table structures of different in-plane dimensions (L), corresponding to the marked points in (c). S1-S3 refer to state 1-3, respectively. Scale bars, 1 cm.

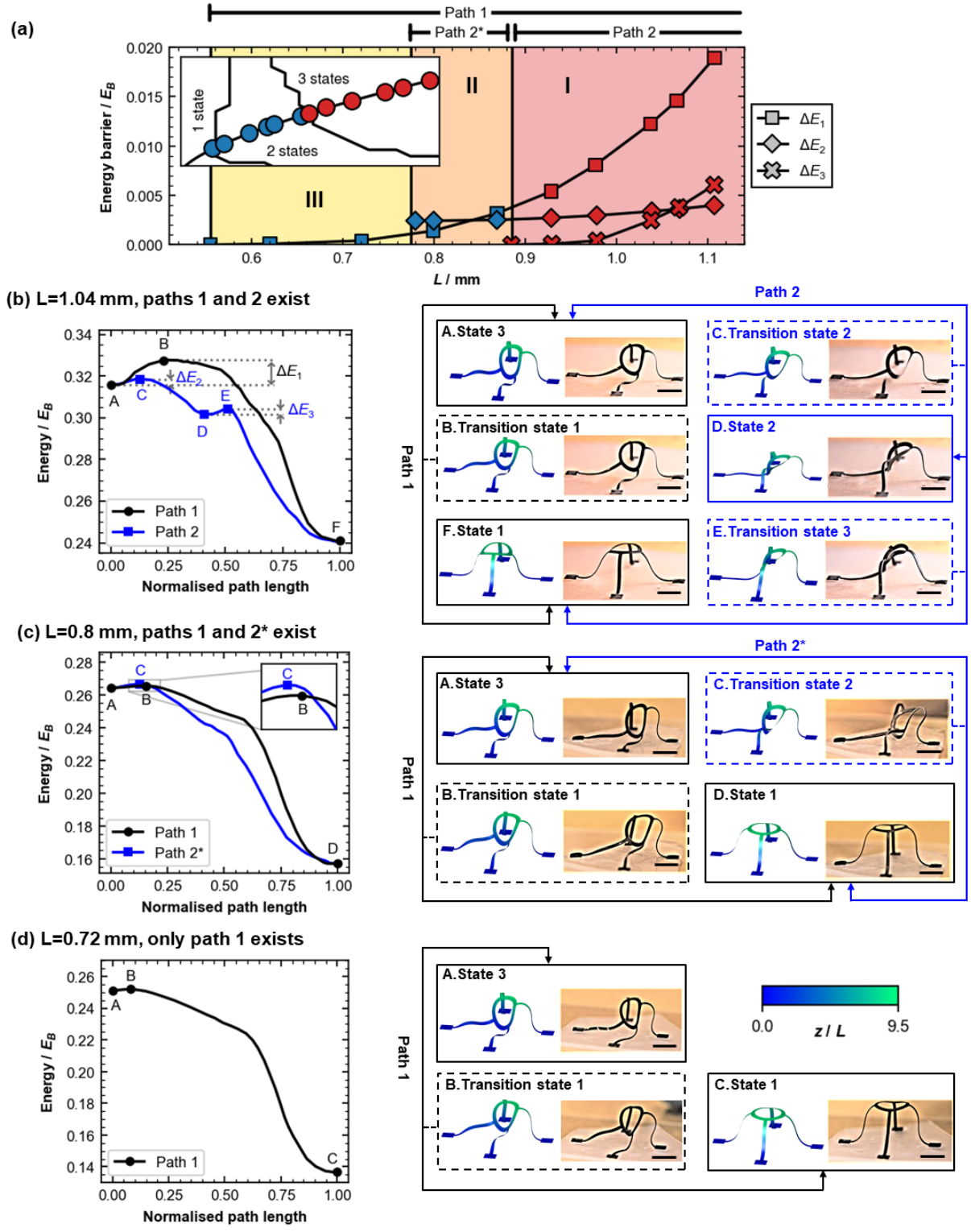

Figure 2. Energy barriers and reconfiguration pathways. (a) Variation of the energy barriers against L. Three regions (I-III) with different available pathways are highlighted. Inset: location within the design phase diagram in Figure 1c for each value of L. **(b-d)** Energy profiles and snapshots of corresponding stable and transition states for reconfiguration pathways from state 3 to 1 with three representative structures: (b) L = 1.04 mm, (c) L = 0.8 mm, and (d) L = 0.72 mm. The energies are normalized by the bending energy. In (b), the definition of the three energy barriers (ΔE_1, ΔE_2, ΔE_3) is defined. Scale bars, 1 cm.

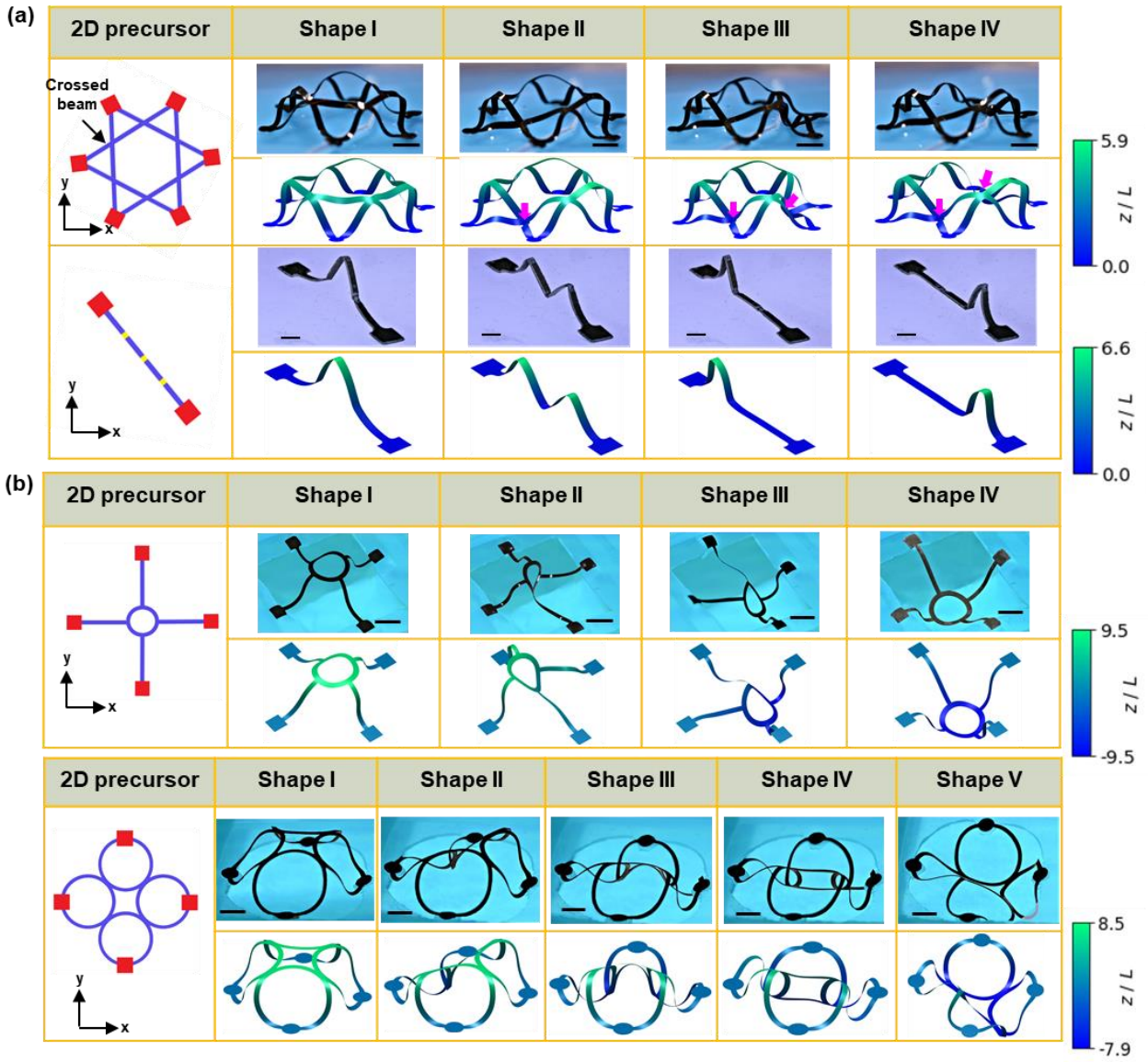

Figure 3. Diverse magnetically reconfigurable 3D structures. Optical images and computational modeling of multistable states for three types of structures: **(a)** 3D structures attached to a substrate. Pink arrows in the first structure indicate differences among the four shapes. Scale bars in the first and second structure are 1 cm and 2 mm, respectively. **(b)** 3D structures with the substrate underneath the structure removed to allow more freedom for reconfiguration. Please note that the structures are placed vertically, with the direction of gravity along the x direction. Scale bars, 1 cm. **(c)** 3D structures composed of locally patterned ferromagnetic films on a thin layer of PDMS. Scale bars, 1 cm.

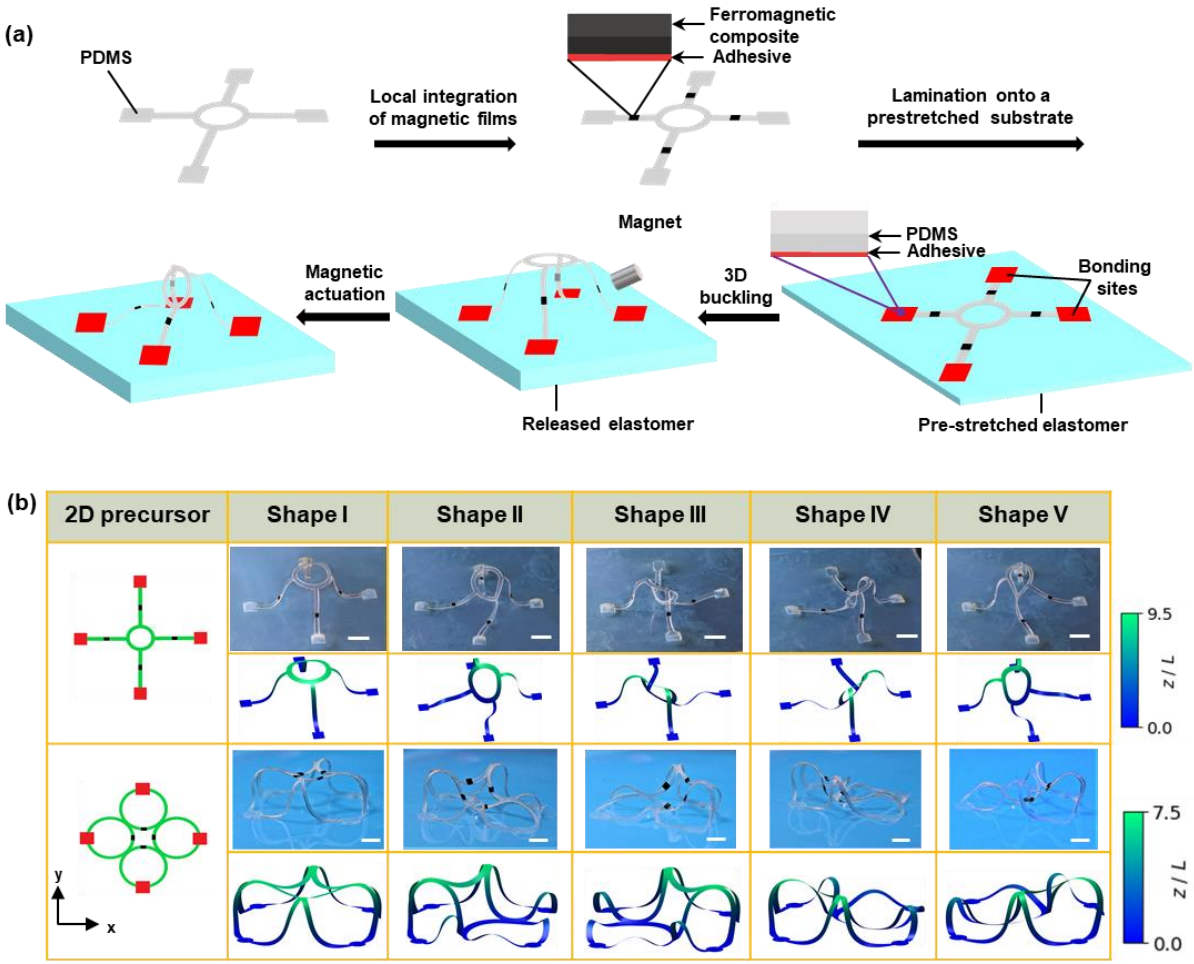

Figure 4. Locally tunable, heterogeneous 3D structures. (a) Schematic illustration of the fabrication process for locally controlled heterogeneous 3D ferromagnetic structures. **(b)** Optical images and computational modeling of multistable states for 3D structures composed of locally patterned ferromagnetic films on a thin layer of PDMS. Scale bars, 1 cm.

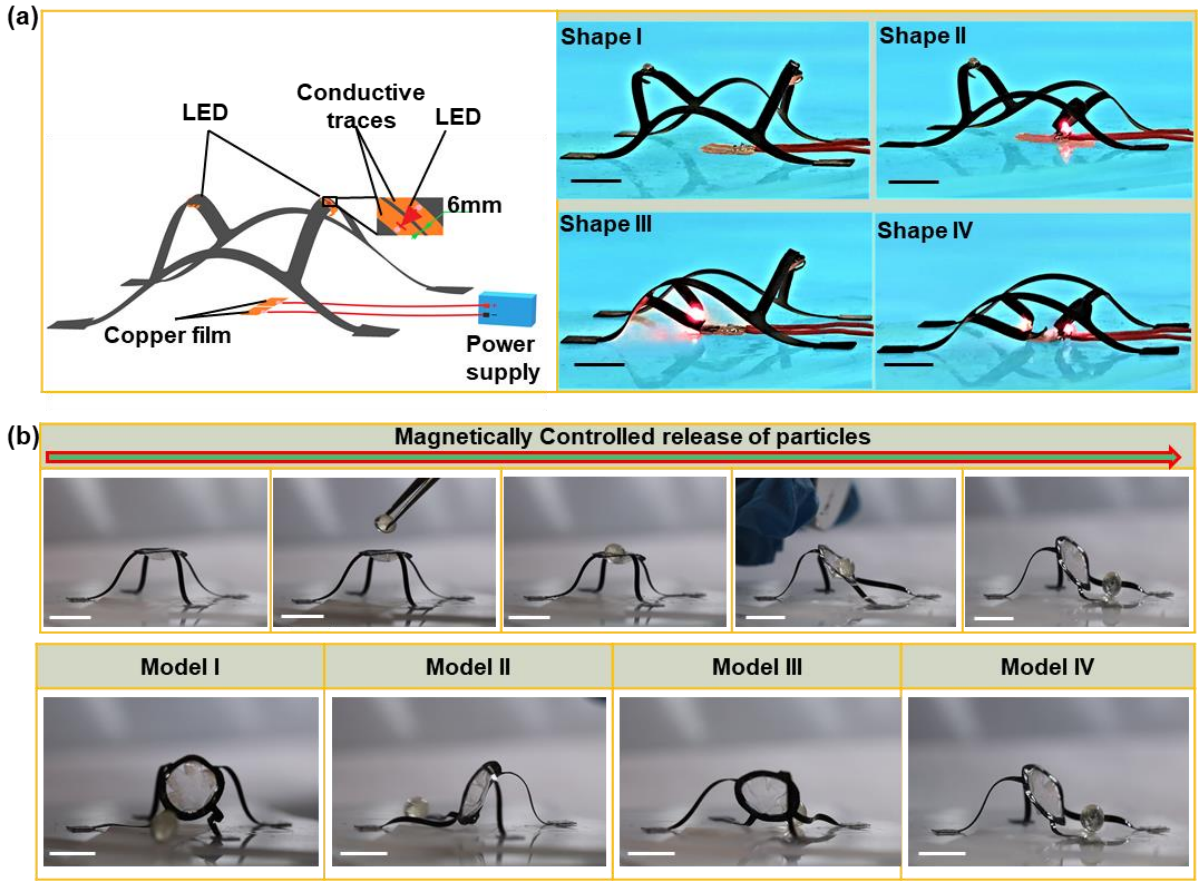

Figure 5. Applications of reconfigurable structures in on-demand 3D light emitting systems and controlled particle delivery. (a) Schematic illustration and optical images of a 3D light emitting system that can be reconfigured among its multistable states to switch the LEDs on and off. Scale bars, 1 cm. **(b)** Controlled release of particles in four different directions (Modes I-IV) enabled by four possible stable states of the table structure. Scale bars, 1 cm.

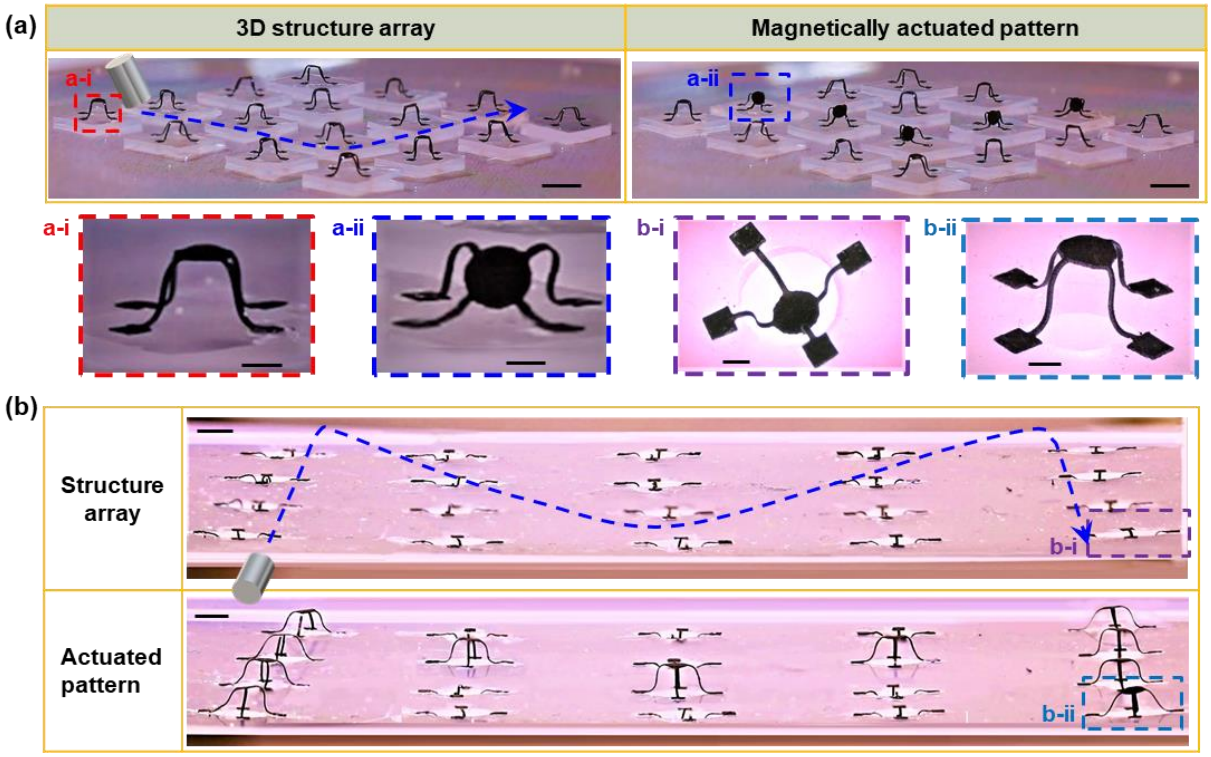

Figure 6. Reconfigurable 3D structure array. (a) A 4×4 array of multistable table structures (on an intact substrate) magnetically deformed to display an alphabetic pattern of "V". Scale bars, 5 mm. Image A-D are magnified views of the 3D structures; Scale bars, 1 mm. **(b)** A 4×5 array of multistable table structures (with the substrate underneath the 3D structure removed) magnetically deformed to display an alphabetic pattern of "M". Scale bars, 3 mm.